Water-Based Synthesis of Zr6-Based Metal–Organic Framework Nanocrystals with Sulfonate Functions: Structural Features and Application to Fructose Dehydration

Bakytzhan Yeskendir, Priscilla Magalhaes de Souza, Pardis Simon, Robert Wojcieszak, Christian Courtois, Yannick Lorgouilloux, Sebastien Royer, Jean-Philippe Dacquin, Jérémy Dhainaut

Water-based Synthesis of Zr_6-based Metal-Organic Framework Nanocrystals with Sulfonate Functions: Structural Features and Application to Fructose Dehydration

Bakytzhan Yeskendir[1,2], Priscilla M. de Souza[1], Pardis Simon[1], Robert Wojcieszak[1], Christian Courtois[2], Yannick Lorgouilloux[2], Sébastien Royer[1], Jean-Philippe Dacquin[1], Jérémy Dhainaut[1,*]

[1] Université de Lille, CNRS, Centrale Lille, Université Artois, UMR 8181 – UCCS – Unité de Catalyse et Chimie du Solide, Lille, 59000, France.

[2] Univ. Polytechnique Hauts-de-France, CERAMATHS – DMP – Département Matériaux et Procédés, F-59313 Valenciennes, France.

*Mail: jeremy.dhainaut@univ-lille.fr.

Abstract

A series of zirconium-based Metal-Organic Framework (MOF) nanocrystals (95-211 nm) displaying sulfonate functions (UiO-66-SO_3H) was prepared in N,N-dimethylformamide (DMF) – the conventional solvent – and water, and their physicochemical properties were thoroughly investigated. In particular, XRD results suggest that upon replacing DMF with water, the resulting MOF crystal structure presents a highly defective structure belonging to the space group *Im-3* instead of the typical *Fm-3m*. The acid catalysts were applied to the fructose dehydration into 5-hydroxymethylfurfural (5-HMF). Complete conversion of fructose over UiO-66-SO_3H prepared in water was reached after only 30 minutes at 100 °C, in line with its stronger Brønsted acidity. In comparison, its counterpart prepared in DMF showed only 30 % fructose conversion. Moreover, intrinsic catalytic effect at 80 °C was only observed with the water-based UiO-66-SO_3H. Without reactivation of the catalyst, recycling tests demonstrated the preservation of its structural integrity upon 9 consecutive cycles, while a gradual loss of the catalyst activity was attributed to the humins adsorption on the MOFs.

Keywords: Metal-organic frameworks, Zr_6 clusters, sulfonate groups, green synthesis, fructose dehydration

1. Introduction

The studies on conversion of biomass into fine chemicals and fuels has significantly increased over the past years highlighting biomass as a sustainable feedstock for the production of a variety of valuable chemicals [1–3]. Lignocellulosic biomass is of particular interest, as it does not compete with food production. Generally, lignocellulosic biomass consists of three major polymeric components: lignin (~25 %), cellulose (~45 %) and hemicellulose (~30 %) [4]. Upon acidic pretreatment, cellulose and hemicellulose are depolymerized into hexoses and pentoses, respectively [5,6]. This step is crucial as it allows to obtain convertible sugar monomers from carbohydrate polymers in a cost-effective way, however technologically challenging at large scale. Other pretreatment technologies include physical (mechanical, ultrasound, microwave), chemical (acid, alkaline), and biological (microbes, enzymes) methods [7]. Thereafter, many reactions may be performed to convert the sugar monomers into more valuable products, such as hydrogenation, isomerization, and deoxygenation [8]. Specifically, fructose is the product of glucose isomerization which is oftentimes catalyzed by enzymes (Figure 1) [9].

One of these particularly interesting reactions is the dehydration of fructose to 5-HMF which is amongst the top-10 platform molecules, building blocks that can be further transformed into a variety of valuable products. For example, further oxidation of 5-HMF leads to the formation of 2,5-furandicarboxylic acid (2,5-FDCA), which is a potential green alternative to terephthalic acid for the production of polyesters, notably polyethylene terephthalate (PET) [10].

Dehydration of fructose to 5-HMF (Figure 1) is a one-step reaction which is usually performed in liquid phase, using various solvents such as water [11], organics [12], biphasic systems [13] and ionic liquids [14]. In addition, different activation approaches have been applied such as conventional [15] and microwave [16] heating.

Generally, dehydration of fructose itself is catalyzed by Brønsted acids. For instance, dehydration of fructose using a HCl/DMSO (dimethyl sulfoxide) mixture at 90 °C reached a conversion of 97 % and a 5-HMF yield of 69 % in 2 h [17]. Similar results were obtained when formic acid was used as the catalyst in a water/n-butanol mixture at 170 °C, with 98 % conversion and 5-HMF yield of 69 % [18]. Currently, the industrial process is based on hydrothermal carbonization (HTC) of sugarcane biomass and gives 5-HMF with a purity as high as 99.9 % for a rough capacity production of 20 tons per year [19]. Albeit both high conversion and yield could be achieved following homogeneous catalytic processes, reactor corrosion and loss of the soluble catalyst from the mixture is particularly problematic.

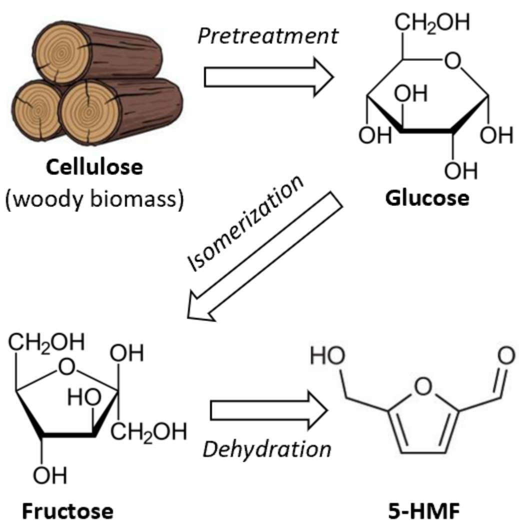

Figure 1. General process pathway towards production of 5-HMF from lignocellulosic biomass.

Apart from mineral and organic acids, a wide variety of solid acid catalysts have been tested in fructose dehydration. Namely, zeolites [20], ion-exchange resins [21] or functionalized porous materials [22] have demonstrated good activity in fructose dehydration. For instance, fructose conversion reached 72 % with 55 % 5-HMF yield over H-beta (Si/Al = 25) nanozeolite after 2 h in DMSO at 120 °C [23]. Likewise, sulfonic acid-grafted mesoporous silica, SBA-15-SO_3H, showed 99 % conversion and 81 % 5-

HMF yield after 1 h at 120 °C in ionic liquid [BMIM]Cl [24]. Complete fructose conversion at 120 °C as well as 100 % 5-HMF yield were obtained in DMSO after 2 h over Amberlyst-15 under continuous evacuation of the released water resulting in an increase of the product yield [25]. Additionally, remarkable 100 % fructose conversion and 93 % 5-HMF yield were obtained also in DMSO after 1 h over Amberlyst-70 at 140 °C [26]. It should be noted that such high temperatures (≥ 120 °C) hinder the cost-efficiency of the overall process. The development of alternative catalysts, allowing to work at mild temperatures, would thus be highly attractive.

Over the past ten years, MOFs have been extensively investigated. Their structure is comprised of metal nodes (ions or clusters) and organic linkers (for example, di- and tricarboxylic acids). Together they form highly crystalline porous solids. Owing to their unique combination of large surface area, controllable pore size as well as high physicochemical properties tunability, they have been used in various applications such as heterogeneous catalysis [27], waste-water purification [28], toxic gas removal [29] and gas storage [30], sometimes even unveiling performances unreachable by conventional porous solids [31].

One of the most famous and well-studied MOFs is the UiO-66 (Universitetet i Oslo) compound. This MOF is composed of $Zr_6O_4(OH)_4^{12+}$ clusters connected by terephthalate linkers to form a continuous 3D structure with a cubic symmetry of the unit cell (*Fm-3m* space group), an approximate surface area of ~1000-1200 $m^2 \cdot g^{-1}$ and pores size below 2 nm [32]. Due to the phenomenon known as “missing linkers”, the classical UiO-66 exhibits Lewis acidity thanks to the Coordinatively Unsaturated Sites (CUS) on Zr-oxoclusters, which can be active in sugar isomerization. Thus, upon isomerization of glucose over UiO-66, fructose yield reached ~35 % at ~50 % glucose conversion at 90 °C in 1-PrOH [33]. However, in order to make the classical UiO-66 highly active in sugar dehydration, Brønsted acid sites and especially sulfonic acid functions should be inserted into the framework of the MOF. Indeed, UiO-66-SO_3H analogues have shown to improve the dehydration activity compared to the non-functionalized UiO-66. Thus, one-pot glucose conversion *via* dehydration of fructose into 5-HMF at 140 °C resulted in an increased 5-HMF yield from 3 % to 8 % upon increasing the content of -SO_3H functions up to 20 wt.% [34].

Similarly, direct fructose dehydration into 5-HMF over MOFs with sulfonic acid functions leads to a considerable increase in conversion and product yield. Thus, the post-synthetic functionalization of MIL-101(Cr) led to complete fructose conversion with 90 % 5-HMF yield in 1 h at 120 °C, whereas the non-functionalized MOF exhibited a fructose conversion of 45 % and 5-HMF yield of 24 % [35].

Currently, one of the main issues for the use of UiO-66 and its functionalized derivatives at industrial scale is that their synthesis often uses DMF, a well-known hazardous and toxic solvent. It is classified as toxic to reproduction, acute toxicant (inhalation and dermal route) and as an eye irritant in accordance with EU Regulation (EC) No 1272/2008. Moreover, DMF could be responsible for severe liver damages upon exposure, provoking hepatitis and cancer [36]. Therefore, there is a need to establish strict regulation rules for the use of DMF. Recently, the European Commission adopted a regulation amending Annex XVII of REACH (Registration, Evaluation, Authorisation and Restriction of Chemicals) to restrict the solvent on the EU market starting from December 2023. DMF remains required for the synthesis of classical UiO-66 as its ligand, terephthalic acid, is insoluble in most conventional solvents. This is the reason why functionalized UiO-66 analogues are also frequently made in DMF [37–39]. Therefore, the replacement of DMF is seen as an essential strategy for MOFs synthesis. To date, a few papers have reported sustainable methods for the preparation of MOFs [40,41].

Particularly, green and scalable syntheses of UiO-66-based functionalized MOFs have been extensively developed within the past few years due to decent solubilities of the functionalized terephthalate linkers in water. Interestingly, the procedures for tuning the chemical properties of conventional porous solids such as zeolites, carbons or silicas is more complex as compared to the MOFs, especially in green conditions. Therefore, the list of UiO-66-X prepared in water includes the following nominations: UiO-66-COOH [42–44], UiO-66-$(COOH)_2$ [43,45–47], UiO-66-$(COOH)_4$ [47], UiO-66-NH_2 [43,44,46,47], UiO-66-NO_2 [48], UiO-66-F_4 [45–47], UiO-66-$(OH)_2$ [43,47], and UiO-66-SO_3H [49].

As evident from Table S1, the variety of functionalized MOFs derived from UiO-66 can be as large as the number of existing terephthalate-derived linkers. Of note, varying the Zr-source also leads to porous MOFs with decent available surface areas. Therefore, the present work is exploring water-based synthesis of UiO-66-SO_3H MOF with emphasis on synthesis condition optimization and the resulting physicochemical properties, as well as its performance in fructose dehydration to 5-HMF with respect to UiO-66-SO_3H prepared in DMF. UiO-66 was chosen as the target MOF due to its good textural properties, thermal and chemical stabilities [50] as well as its chemical properties tunability [37,51]. Direct recyclability of the water-based UiO-66-SO_3H over subsequent runs, which simulates to some extent its use in a continuous process using batch conditions, was also investigated.

2. Experimental

2.1 Materials

Zirconium chloride (99.5 %, Alfa Aesar), zirconium sulfate tetrahydrate (98 %, Alfa Aesar), terephthalic acid (99 %, Acros Organics), monosodium 2-sulfoterephthalate (98 %, TCI Chemicals), D-fructose (99 %, Acros Organics), N,N-dimethylformamide (pure, Carlo Erba Reagents), dimethyl sulfoxide (99.7 %, Fisher BioReagents), acetic acid (100 %, VWR), ethanol (96 %, VWR), and 5-(hydroxymethyl)furfural (98 %, Acros Organics) were used as-received.

2.2 Catalysts preparation

UiO-66 was synthesized following the methodology previously described by Foo *et al.* [37]. Namely, 0.32 g of $ZrCl_4$ and 0.22 g of terephthalic acid (molar ratio of 1:1) were dissolved in 100 mL of DMF. Upon dissolution, 3 mL of acetic acid were added and thereafter the entire solution was placed in the PTFE (polytetrafluoroethylene) liner of a stainless-steel autoclave and heated at 120 °C for 24 h. After crystallization, a white solid product was recovered by centrifugation and washed in fresh DMF at 50 °C to dissolve unreacted species. This was followed by 3 consecutive washing steps in ethanol at 50 °C. Eventually, the product was recovered and dried overnight at 100 °C.

The preparation of UiO-66-SO_3H-D was done similarly, by dissolving 0.31 g of $ZrCl_4$ and 0.35 g of monosodium 2-sulfoterephthalate (molar ratio of 1:1) and adding acetic acid in 100 mL of DMF. All other steps are identical as in the case of UiO-66. For comparison, a material with a molar ratio of 1:2 was also prepared.

For UiO-66-SO_3H-W preparation, 1 g of $Zr(SO_4)_2{\cdot}4H_2O$ and 1.44 g of monosodium 2-sulfoterephthalate (molar ratio of 1:2) were dissolved in 100 mL of water. The resulting solution was heated up to 100 °C under reflux, as a simpler alternative to solvothermal conditions. The resulting white solid was recovered and washed 3 times with fresh H_2O as well as with ethanol at 50 °C overnight. Upon washing, the product was dried at 100 °C overnight. For comparison, materials with a molar ratio of 1:1 and with either $ZrCl_4$ or $Zr(SO_4)_2{\cdot}4H_2O$ were also prepared.

2.3 *Catalysts characterization*

Powder X-Ray Diffraction (XRD) patterns were recorded on a D8 Advance instrument from Bruker, equipped with a CuK_{α} X-ray source (λ = 1.54184 Å), using the following parameters: 2θ range between 5-40 °, scan rate of 0.02 °/step, and acquisition time of 1 s/step. The simulated pattern of UiO-66-SO_3H was plotted using its CIF file provided by Taylor *et al.* [49].

Textural properties were measured by N_2 physisorption experiments performed at 77 K using a Micromeritics Tristar II instrument. Before analysis, a known mass (~ 50 mg) of solid was treated at 120 °C under vacuum for 15 h. Specific surface area (S_{BET}) was calculated using the B.E.T. method, on the linear part of the B.E.T. plot (p/p_0 = 0.1-0.3). Pore volume was calculated using the adsorption branch of the isotherms at a p/p_0 value of 0.99. Pore size distribution from 1.0 nm was given by the non-local density functional theory (NLDFT) model.

Scanning electron micrographs were registered on a JEOL JSM 6700F microscope in the range of 5-10 kV. Before observation under microscope, the samples were covered with a thin layer of Cr (150 Å).

Infrared spectra (IR) were measured on a Perkin–Elmer "Spectrum Two" spectrometer equipped with a diamond and operating in the attenuated total reflectance (ATR) mode between 4000 and 400 cm^{-1}.

Raman spectra were recorded on an XPlora Plus from Horiba Scientific micro-spectrometer equipped with a 50X focal length objective. The acquisition of spectra was performed using a laser excitation wavelength of 532 nm and a 50 % filter to avoid possible sample degradation under the laser beam.

X-ray Photoelectron Spectroscopy (XPS) analysis was performed on a Kratos Axis Ultra DLD instrument equipped with a monochromatized AlK_{α} X-ray source powered at 225 W (15 mA, 15 kV). The base pressure in the analysis chamber was lower than 5.10^{-9} Torr. General survey spectra were recorded at a 160 eV pass energy and Zr 3d, C 1s, O 1s and S 2p core level spectra were recorded at a 20 eV pass energy. The Kratos charge compensation system was used during all analysis, and Binding Energy (BE) scales were adjusted according to the Zr $3d_{5/2}$ peak placed at 182.8 eV. The relative surface atomic quantification was obtained after the subtraction of a Shirley type background on all spectra.

Thermogravimetric analysis (TGA) profiles were obtained with a thermal analyzer instrument Q600 from TA Instrument within the temperature range 25 – 800 °C at a heating rate of 5 $°C·min^{-1}$ in air flow (100 $mL·min^{-1}$).

Chemical composition of the catalysts was determined by Inductively Coupled Plasma – Optical Emission Spectroscopy (ICP-OES). Analyses were performed on a Perkin Elmer Optima 2000 DV instrument to determine the chemical composition of the solids based on Zr, S and Na. Before analysis, a known amount of sample was dissolved in a diluted HF-HCl solution, and then heated under microwave until complete dissolution.

Acid site density of the catalysts was estimated by acid-base titration method. For this, 0.1 g of solid was immersed into 100 mL of 1M $NaNO_3$ solution and left overnight under constant stirring. This step was repeated 3 times. After that, the mixture was centrifugated and a 50-mL aliquot was titrated with 0.01 M NaOH solution using phenolphthalein as color indicator [35].

2.4. Catalytic tests

Fructose dehydration reaction was performed in a Carousel 12 Plus Reaction Station from Radleys, working at atmospheric pressure, using 1.2 mmol of fructose, 2 mL of DMSO and 20 mg of catalyst. The reaction mixture and the catalyst were stirred at 600 rpm and heated to the desired reaction temperature (80-120 °C) with a reaction time up to 6 h. At the end of the reaction, the reactors were cooled to room temperature and the products were removed with a syringe, filtered and diluted 10 times using a 5 mM sulfuric acid solution. The products were analyzed in high-performance liquid chromatography (HPLC) equipped with UV-vis and refractive index (RID) detectors and a Rezex ROA-Organic Acid column using sulfuric acid (5 mM, 0.6 mL·min^{-1}) as a mobile phase. For the recycling experiments, the catalyst was separated by centrifugation and then reused directly for the next run with a fresh fructose solution in DMSO. The fructose conversion and 5-HMF yield were defined as:

$$\boldsymbol{Conversion}\ (\%) = \frac{\textbf{mol of Fructose}_{\boldsymbol{i}} - \textbf{mol of Fructose}_{\boldsymbol{f}}}{\textbf{mol of } \boldsymbol{Fructose_i}} \quad (1)$$

$$\boldsymbol{Yield}\ (\%) = \frac{\textbf{mol of HMF}}{\textbf{mol of } \boldsymbol{Fructose_i}} \quad (2)$$

3. Results and discussion

3.1. Catalyst characterization

Figures 2.a and S1 show the XRD patterns of the as-synthesized UiO-66 and the sulfonate-functionalized MOFs prepared in DMF (UiO-66-SO_3H-D) or in water (UiO-66-SO_3H-W). It appears that a ratio of 1:2 was necessary to obtain a highly crystalline sulfonic-functionalized MOF in water, while from a ratio of 1:1 the obtained UiO-66 and UiO-66-SO_3H-D were of similar crystallinity. Owing to the difficulty to activate MOFs with large amounts of linkers trapped within their porosity, only the ratio of 1:1 will be considered next for the MOFs synthesized in DMF. As expected, the prepared UiO-66 exhibits characteristic reflections at approximately 7.4, 8.4 and 25.5 ° (2θ) corresponding to the (111), (002) and (006) planes, respectively [32]. A similar XRD pattern was obtained for UiO-66-SO_3H-D implying that, using DMF as solvent, the presence of -SO_3H groups does not change the topology of the resulting MOF: a face-centered cubic organization in the unit cell (*Fm-3m* space group, a = 20.7004 Å). Interestingly, the pattern of UiO-66-SO_3H-W obtained after 24 h of crystallization time exhibits several additional reflections. Indeed, when synthesized in water, UiO-66-SO_3H adopts a unique topology representing a cubic organization with a doubled unit cell parameter (*Im-3*, a = 41.4906 Å) and a lowered crystallographic symmetry [49,52]. This phenomenon is related to a large number of structural defects, with only 8 linkers coordinating the Zr_6 clusters instead of 10 to 12 [49]. Then, upon changing the solvent from DMF to water, a UiO-66-SO_3H MOF with slight differences in terms of physico-chemical properties was obtained. Especially, due to its defective framework, higher textural properties are expected. Of note, few authors attributed a different name to the resulting MOF structure: NUS-6 [53].

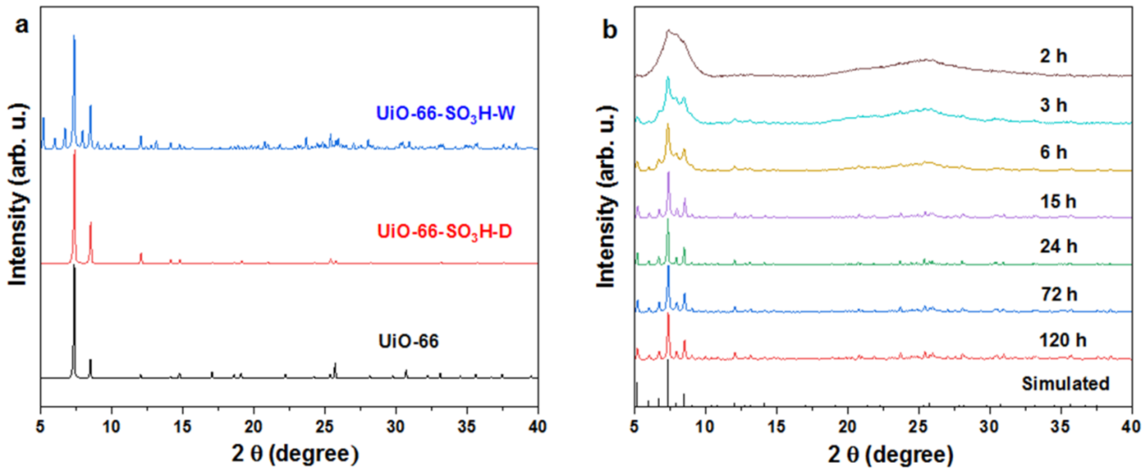

Figure 2. XRD patterns of UiO-66, UiO-66-SO_3H-D and UiO-66-SO_3H-W (a) and UiO-66-SO_3H-W prepared in water with various synthesis durations (b).

To optimize the preparation of UiO-66-SO_3H-W, crystallization kinetics was studied at 100 °C and the related XRD diffractograms are displayed in Figure 2.b. Semi-crystalline solids yielding broadened reflections can be observed from 3 h, and upon 15 h the MOF crystallization process was complete as the obtained solids possessed well-defined reflections in line with the simulated pattern.

Such tendency is in agreement with the results obtained by N_2 porosimetry analysis. N_2-sorption isotherms are given in Figure S2 and the related data are provided in Table S2. A successive increase of adsorbed N_2 in the micropore region is observed upon crystallization time, hence leading to higher available surface areas and confirming the obtention of better crystallized microporous materials. Of note, a small N_2 uptake at high partial pressures (p/p_0) indicates the presence of intercrystalline porosity which is generally observed with small crystals. Owing to its decent yield and S_{BET}, only the UiO-66-SO_3H-W prepared within 24 h will be considered hereafter.

The impact of the linker and the type of solvent over the final textural properties can be deduced from N_2 physisorption isotherms depicted in Figure 3. The type I adsorption/desorption isotherms, with a plateau at low relative pressures ($p/p_0 < 0.2$) for all studied solids, are characteristic of microporous materials. The slight uptake observed at high relative pressure ($p/p_0 > 0.9$) is typical of intercrystalline porosity for nanomaterials. Furthermore, the presence of sulfonic acid functions may be deduced from the significantly lower nitrogen adsorbed at any partial pressure, as the functions occupy an important space within the porosity of the MOF. As seen in Table 1, the non-functionalized UiO-66 exhibits the highest specific surface area (1206 $m^2 \cdot g^{-1}$) and micropore volume (0.47 $cm^3 \cdot g^{-1}$) as opposed to the UiO-66-SO_3H materials. The synthesis of UiO-66-SO_3H in DMF leads to a significant decrease of about 60 % in specific surface area (468 $m^2 \cdot g^{-1}$) and micropore volume (0.19 $cm^3 \cdot g^{-1}$). Of note, Biswas *et al.* also prepared UiO-66-SO_3H in DMF and obtained a specific Langmuir surface area of 769 $m^2 \cdot g^{-1}$ and a micropore volume of 0.26 $cm^3 \cdot g^{-1}$ [39]. Herein, when DMF is replaced by water, a micropore volume of 0.26 $cm^3 \cdot g^{-1}$ is also obtained along with a BET surface area of 639 $m^2 \cdot g^{-1}$ (-47 % as compared to the reference UiO-66) after 24 hours of crystallization time. After 72 hours, the resulting BET surface area (630 $m^2 \cdot g^{-1}$) remains within the experimental and apparatus errors (± 5 $m^2 \cdot g^{-1}$). Regarding the pore size distribution, from 1 nm all materials display similar pore widths centered around 1.25 nm and 1.50 nm (Figure S3). UiO-66-based MOFs should also present a pore width centered around 0.6 nm [32], which could not be probed by the apparatus used. Therefore, the use of a modulator (acetic acid) or the replacement of DMF by water result in mostly comparable specific surface areas, microporous volumes and pore widths for both sulfonate-functionalized MOFs, but with an expected drop as compared to the original UiO-66 due to the presence of bulky sulfonate moieties.

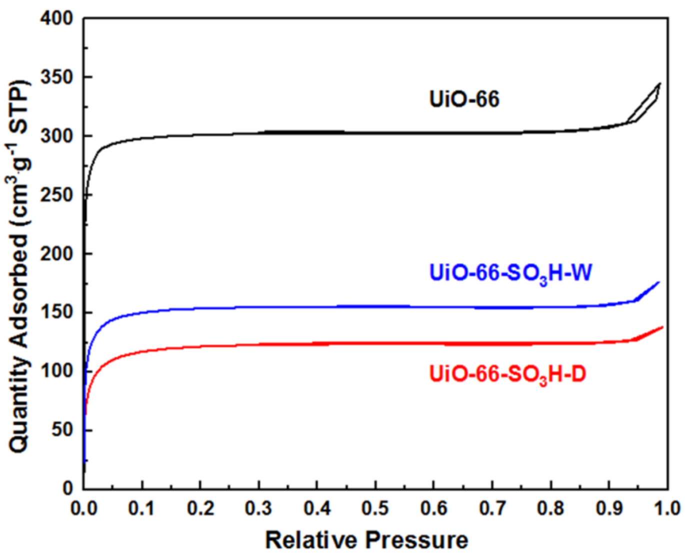

Figure 3. N_2 physisorption isotherms of the UiO-66-based catalysts.

The Brønsted acidity of both UiO-66-SO_3H was estimated *via* acid-base titration method. UiO-66-SO_3H-W presents an increased acid sites density as compared to its counterpart prepared in DMF (0.77 $mmol \cdot g^{-1}$ *vs* 0.49 $mmol \cdot g^{-1}$). The higher available surface area of the former does not fully support this increase, as the acid sites density remains 15 % higher when expressed in $\mu mol \cdot m^{-2}$ (Table 1). This either implies that some acid sites are inaccessible, or that more linker defects are present in UiO-66-SO_3H-D due to lower Zr:linker ratio used for its synthesis. Besides, post-modification of UiO-66 into UiO-66-SO_3H in the reference work by Chen *et al.* [35] led to an acid sites density of

0.41 mmol·g^{-1}, underlining that direct synthesis seems a better method to obtain more acidic catalysts.

Table 1. Textural and acid properties of the as-synthesized MOFs.

Catalysts	S_{BET} ($m^2·g^{-1}$)	V_{total} ($cm^3·g^{-1}$)^a	V_{micro} ($cm^3·g^{-1}$)	Acid sites density^b ($mmol·g^{-1}$)	($\mu mol·m^{-2}$)
UiO-66	1206	0.53	0.47	-	-
UiO-66-SO_3H-D	468 (-61 %)	0.21 (-60 %)	0.19 (-60 %)	0.49	1.05
UiO-66-SO_3H-W	639 (-47 %)	0.27 (-49 %)	0.26 (-45 %)	0.77	1.21

^{a} Derived from adsorption branch of isotherms at $p/p_0 = 0.99$;

^{b} Estimated by acid-base titration.

Direct evidence of -SO_3H groups presence on the surface of MOFs is given by FTIR-ATR and Raman spectra shown in Figure 4. Firstly, the bands corresponding to the principal vibrations of the UiO-66 framework are present in all the studied solids. Namely, the IR bands at ~1388 cm^{-1} and 1587 cm^{-1} are characteristic of symmetric and asymmetric stretching mode of ν(O-C-O) in the terephthalate linker, respectively. While its asymmetric mode is inactive in Raman, the symmetric mode is viewed as the "doublet" band at 1427 cm^{-1} and 1450 cm^{-1} in UiO-66 and as an overlapped band in both UiO-66-SO_3H-D and UiO-66-SO_3H-W. The small IR band at 1508 cm^{-1} stem from ν(C=C) of the benzene ring which corresponds to the intense band at ~1615 cm^{-1} in the Raman spectra. Moreover, there are IR bands below 1000 cm^{-1} corresponding to a combination of vibrations: C-H (745 cm^{-1}), μ_3-O (~640 cm^{-1}) stretching [32]. A small shift of the IR and Raman bands on UiO-66-SO_3H-D and UiO-66-SO_3H-W spectra towards higher wavenumbers as compared to the classical UiO-66 might be due to the presence of -SO_3H groups. Importantly, both functionalized UiO-66-SO_3H-D and UiO-66-SO_3H-W exhibited new IR bands that correspond to S-O vibrations (~620 and 1070 cm^{-1}) and S=O vibrations (~1170 and 1233 cm^{-1}), which are coherent with the Raman bands at 1025 cm^{-1} and 1080 cm^{-1}, respectively [35,54]. Besides, the Raman bands at 1140 and 858 cm^{-1} correspond to the breathing mode of the linker and C-H in-plane bending, respectively. Importantly, there is also the IR band characteristic of C=O stretching at ~1665 cm^{-1} in both UiO-66 and UiO-66-SO_3H-D, which allows tracing DMF by its carbonyl group [55]. Thus, this reveals the presence of residual DMF in the pores of these MOFs despite a rigorous activation step, especially in the case of UiO-66-SO_3H-D and even after drying under vacuum (Figure S4). This may be due to the presence of bulky sulfonate moieties, reducing the diffusion within the porosity. Of note, the presence of DMF contributes to lower the specific surface area and the estimated amount of acid sites, as compared to the DMF-free UiO-66-SO_3H-W.

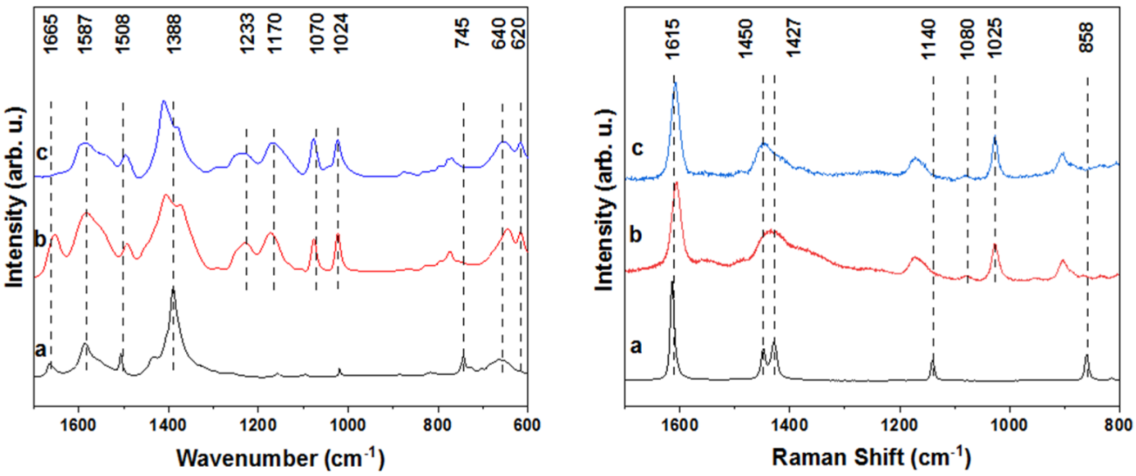

Figure. 4 FTIR-ATR (left) and Raman (right) spectra of the synthesized MOFs: a – UiO-66, b – UiO-66-SO_3H-D, c – UiO-66-SO_3H-W.

The crystal morphology of all the studied materials was visualized by SEM, and representative images are given in Figure S5. The classical UiO-66 is constituted of well-faceted, octahedrally-shaped nanocrystals with a narrow particle size distribution around 132 nm. At the same time, the two sulfonated analogues exhibit distorted nanocrystals inhomogeneous in shape and with an average size above that of UiO-66, as reported in

Table 2. This distortion can be attributed to the presence of $-SO_3H$ groups within the MOF frameworks.

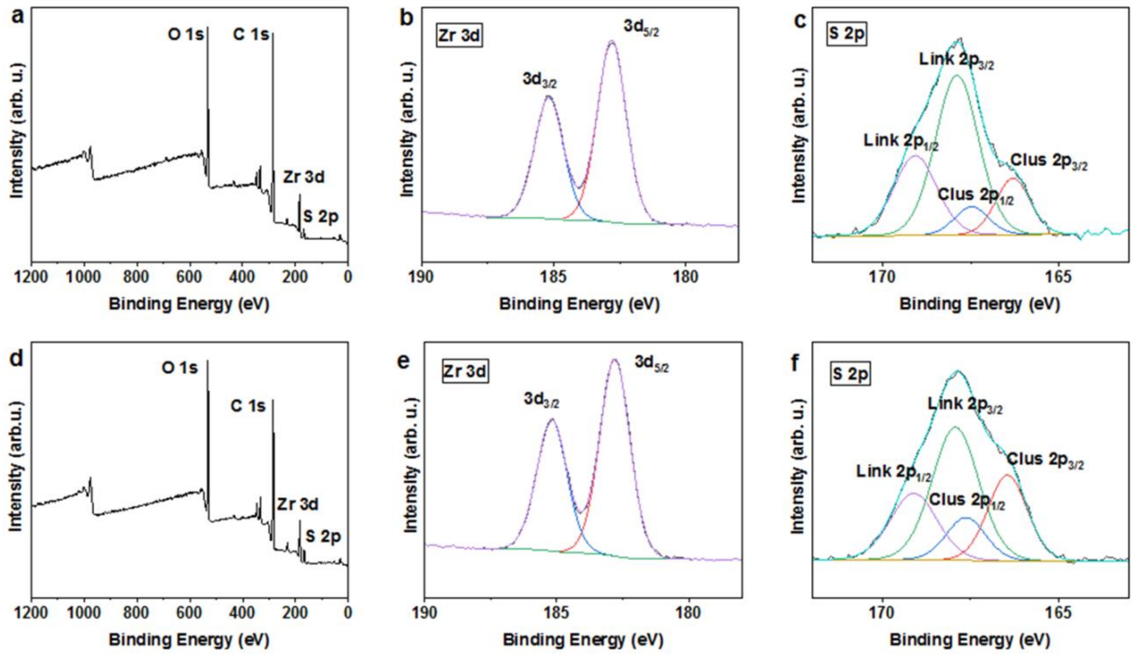

Figure 5. XPS spectra of the as-synthesized solids: UiO-66-SO_3H-D survey (a), Zr 3d (b) and S 2p (c) as well as UiO-66-SO_3H-W survey (d), Zr 3d (e) and S 2p (f).

It has been evidenced that UiO-66 MOFs are prone to structural defects estimated from the number of missing linkers. A rough estimation of the latter was made *via* TGA measurements (Figure S6) using a method described by Shearer *et al.* [56]. Accordingly, the classical UiO-66 exhibited one missing terephthalate ligand per Zr_6-cluster while the two functionalized MOFs surprisingly exhibited approximately 2.3 missing ligands per cluster. These results were further supported by ICP elemental analysis, according to which UiO-66-SO_3H-D and UiO-66-SO_3H-W had 1.51 and 1.41 zirconium atoms per sulfur atom, respectively. This, in turn, suggests that UiO-66-SO_3H-D would actually be slightly more defective than UiO-66-SO_3H-W, owing to the large concentration of modulators (acetate from acetic acid and formate from DMF degradation) in the synthesis mixture. Accordingly, the Zr/S surface atomic ratios derived from XPS analysis of UiO-66-SO_3H-D and UiO-66-SO_3H-W are 1.60 and 1.46, respectively (Figure 5). This agrees well with previous studies [49]. The resulting molecular formula of UiO-66-SO_3H-W is thus $Zr_6O_4(OH)_4[C_6H_3(COO)_2SO_3H]_{4,3}$.

Table 2. Crystallite and particle sizes, and sulfur content of the as-synthesized catalysts.

Catalysts	**D_c(nm)[a]**	**D_p(nm)[b]**	**Zr/S atomic ratio**		**Missing linkers**
			ICP	**XPS[c]**	**per Zr-cluster[d]**
UiO-66	95	132	-	-	0.9
UiO-66-SO_3H-D	98	183	1.56	1.60	2.3
UiO-66-SO_3H-W	105	211	1.41	1.46	2.3

[a] Average crystallite size determined using Scherrer's equation applied to the (111) and the (002) planes; [b] Average particle size measured by SEM; [c] Only the -SO_3H component from S 2p spectra was taken into account to calculate the ratio; [d] Determined by TGA.

Examination of UiO-66 S 2p (Figure S7) spectrum reveals that in this material, which is free of -SO_3H moieties, sulfur traces were found. The spectrum was decomposed into one doublet peak with a S $2p_{3/2}$ - S $2p_{1/2}$ energy splitting of 1.18 eV and a S $2p_{3/2}$ BE centered at 166.9 eV. This contribution is attributed to a Cluster-bound sulfur from impurities.

S 2p spectra of both UiO-66-SO_3H-W and UiO-66-SO_3H-D are decomposed into two doublet peaks with a S $2p_{3/2}$ - S $2p_{1/2}$ energy splitting of 1.18 eV. These two contributions have their S $2p_{3/2}$ BE centered at 166.5 eV and 167.9 eV. The low BE contribution is attributed to cluster-bond sulfur (noted "Clus" on the spectra), whereas the doublet peak with high BE (noted "Link" on the spectra) is consistent with sulfonate moieties (-SO_3H groups) adjacent to aromatic rings [57]. This latter contribution was used to calculate the Zr/S atomic ratios.

As higher BE is directly related to higher positive oxidation states, it is reasonable to hypothesize that the acid strength of the low BE sulfur species is lower. Still, it may impact the acid titration as it is not selective toward sulfonate moieties. Especially, the relative proportion of S species bound to Zr_6-clusters seems higher in UiO-66-SO_3H-W as compared to UiO-66-SO_3H-D, which could be due to the use of zirconium sulfate as a synthesis precursor. Lastly, supported by the absence of a contribution centered at 1071.5 eV on the survey spectra, no sodium was detected implying the complete *in-situ* -SO_3Na to -SO_3H ion-exchange during synthesis, responsible for the Brønsted acidity.

3.2. Fructose dehydration tests

Fructose dehydration to 5-HMF in DMSO at 100 ºC was evaluated using UiO-66, UiO-66-SO_3H-D and UiO66-SO_3H-W as solid catalysts. Figure 6 shows the conversion of fructose as a function of reaction time for all the catalysts as well as for the blank test (without catalyst). Indeed, according to the literature both DMSO and Brønsted acid sites are able to convert fructose to 5-HMF at 100 °C [35,58]. Notably, the two catalysts prepared in DMF (UiO-66 and UiO-66-SO_3H-D) exhibited approximately the same conversion profiles as the blank test, indicating that they possess a low activity under these reaction conditions. Instead, UiO-66-SO_3H-W catalyst achieved the complete conversion of fructose (> 98 %) already after 30 minutes confirming its superior activity, while it remained around 20 % for UiO-66, 30 % for UiO-66-SO_3H-D catalysts and 45 % in DMSO alone.

The presence of residual DMF within the porosity of UiO-66-SO_3H-D, as detected by FTIR spectroscopy, may hinder fructose from reaching the Brønsted acid sites. Especially, DMF was always present on the chromatograms upon analyzing the reaction products when the MOFs prepared in DMF were used as catalysts, while it was absent when using UiO-66-SO_3H-W (Figure S8). An additional blank test was conducted with a mixture of DMSO and DMF (3:1 v:v). As a result, no fructose was converted after 2 h at 100 °C in the presence of DMF, as supported by the colorless reaction solution, while 80

% of fructose was converted in DMSO alone yielding a light-brown colored solution characteristic of 5-HMF presence (Figure S9). Studies on binary mixtures showed that there is a complexation behavior of DMSO-DMF mixture *via* H-bond interactions through S and O atoms on DMSO over a wide range of concentrations [59]. The decreased initial fructose conversion rates over UiO-66 and especially UiO-66-SO_3H-D may hence be attributed to the release of DMF in the mixture. Nevertheless, as it is evident from Figure 6 after 2 h, fructose conversion over UiO-66-SO_3H-D surpasses that of the blank test (98 % *vs* 83 %), and the calculated overall rate constant is higher (Figure S10 and Table S3), highlighting the positive effect of acidic -SO_3H groups on fructose dehydration. In all cases, 5-HMF is identified as the major product, with only traces of an unknown product (Figure S8).

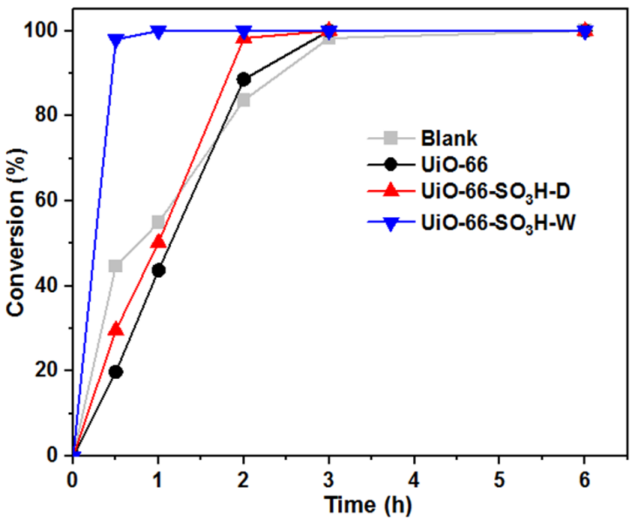

Figure 6. Conversion of fructose at 100 °C as a function of reaction time over different catalysts (UiO-66, UiO-66-SO_3H-D and UiO-66-SO_3H-W) and blank test (without catalyst).

Although UiO-66-SO_3H-W is the most efficient catalyst of the series for converting fructose into 5-HMF, the suppressive effect of DMF present in the catalysts prevent from discussing the effect of the acid site density. While the objective of this study is to prepare environmentally-friendly catalysts for the production of 5-HMF, it should be stressed that the presence of residual DMF should always be assessed prior to dehydration tests.

3.2.1. Effect of reaction temperature

The effect of temperature (80-140 ºC) on the performance of the catalysts in fructose dehydration was further evaluated over UiO-66-SO_3H-W. Figure 7 compares the fructose conversion and yield of 5-HMF after 30 min of reaction carried out with or without UiO-66-SO_3H-W at different temperatures. Furthermore, the related full kinetic profiles are shown in Figure S11.

As expected, the increase of temperature improves the conversion of fructose even when considering only the DMSO solvent (blank tests). At 140 ºC, for example, full fructose conversion was observed already after 30 min of reaction in both cases - blank and with the catalyst. Furthermore, the liquids after reaction showed an intense brown color, in spite of a similar amount of 5-HMF, approximately 75 % of yield. A significant part of the remaining 25 % are constituted of soluble fructose oligomers and insoluble humins which are undetectable by HPLC. These compounds are formed from both fructose and 5-HMF [60].

When the reaction temperature is decreased to 80 ºC, the solvent does not contribute anymore to fructose conversion (blank test) after 30 min (Figure 7). Interestingly, UiO-66-SO_3H-W retains a decent 48 % conversion and 18 % 5-HMF yield. Moreover, it converts 80 % fructose and yields 50 % 5-HMF after 3 h while the blank test still shows no conversion, further proving the catalytic effect of the sulfonic acid groups present in the UiO-66-SO_3H-W catalyst (Figure S11). Finally, after 6 h of reaction at 80 °C, the maximum fructose conversion was 41 % for blank test and 94 % for UiO-66-SO_3H-W with 5-HMF yields of 14 % and 66 %, respectively. Thus, in order to better evaluate a catalyst’s performance in fructose dehydration using DMSO as solvent, it is proposed to apply rather mild conditions *i.e.* 80 °C (or less) for a maximum duration of 3 h. These conditions would allow to neglect the effect of DMSO and attribute fructose conversion as well as 5-HMF yield to the solid acid catalyst only. For higher temperatures, the 5-HMF yield increased quickly with a maximum reached after 2 h, 30 min and 30 min for reactions performed at 100, 120 and 140 °C, respectively (Figure S11).

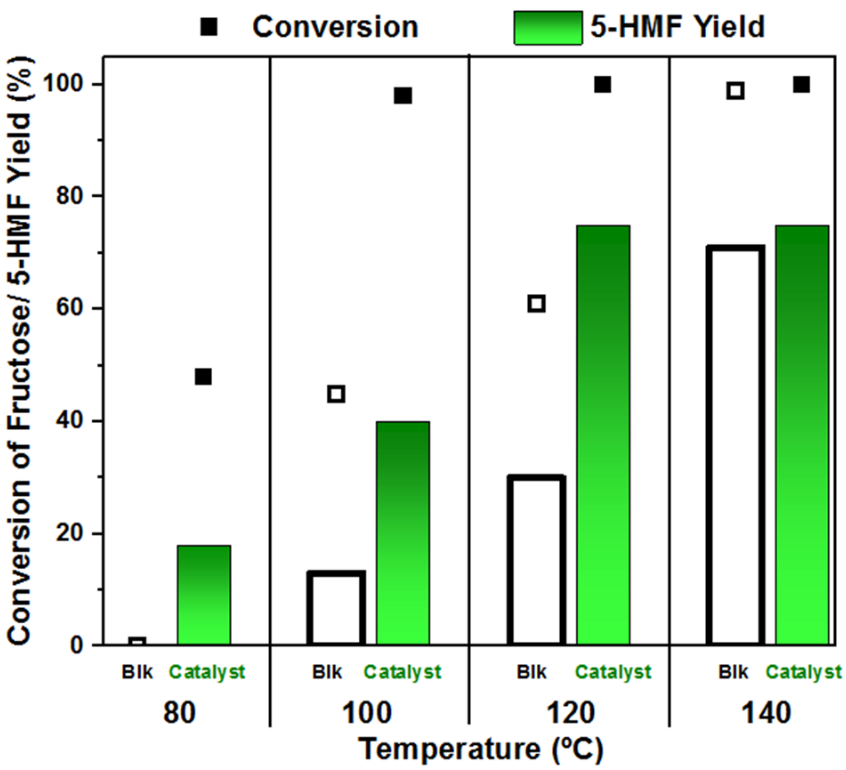

Figure 7. Conversion of fructose and yield of 5-HMF for reactions at different temperatures (30 min). Blk: Blank test; Catalyst: UiO-66-SO_3H-W.

As evident from Table S4, most of the published results on fructose dehydration over MOFs used temperatures of 100 °C and above, which indubitably favor the impact of the DMSO solvent over the catalytic conversion of fructose. In this work, we showed the possibility to reach complete fructose conversion at lower catalyst loading (215 mg fructose : 20 mg catalyst) and temperatures (> 94 % at 80 °C after 6 h).

Interestingly, in the reference work [35], fructose conversion over UiO-66-SO_3H reached ~85 % with a 5-HMF yield of ~70 % in 30 min at 120 °C as compared to 100 % and 76 % respectively in this work. This demonstrates a higher fructose conversion over UiO-66-SO_3H-W prepared *via* direct synthesis as compared to the post-synthesis modification applied in [35], originating from the difference in the sulfonic acid groups concentration. Moreover, faster reaction rates might be obtained using the UiO-66-SO_3H-W catalyst, as 30 min are sufficient to reach fructose conversion and 5-HMF yield in the range of the results reported at 100 °C after 1 h. Only one previous study, using NUS-6 (highly defective UiO-66-SO_3H), presented better results but with a stoichiometric catalyst:fructose ratio [53].

Finally, the structural integrity of UiO-66-SO_3H-W, as viewed from XRD patterns in Figure S12, is preserved upon 6 h of catalytic tests up to 120 °C as all diffractograms conserved the ensemble of characteristic reflections of the as-made UiO-66-SO_3H-W. This implies a decent structural stability upon fructose dehydration in DMSO at high temperatures.

3.2.2. Catalyst recycling

In order to further evaluate the stability and reusability of UiO-66-SO_3H-W, nine runs with the same catalyst were performed at 80 ºC and 100 °C for 30 min. Figure 8 shows fructose conversion and 5-HMF yield after each run. These conditions were chosen in order to eliminate the solvent effect so that the activity can be only attributed to the catalyst.

After nine runs at 80 °C, fructose conversion and yield of 5-HMF reduced gradually from 48 to 25 % and from 18 to 3 %, respectively (Figure 8.a). Notably, from the third run, 5-HMF yield dropped to negligible 3 %, similar to that of the blank test run under the same conditions. The decrease of catalytic activity is typically attributed to the adsorption of humins on the catalyst, hindering access to the active sites. Herein, their presence is supported by FTIR-ATR analysis on UiO-66-SO_3H-W before and after 9 cycles at 80 °C (Figure S13). The spectra demonstrate a new broad band at ~1668 cm^{-1} which corresponds to C=C bond stretching in a furanic ring attributed to humins, while the bands at ~951 and 1004 cm^{-1} might be indicative of adsorbed 5-HMF species on the catalyst surface [61]. Moreover, remarkable deposition of humins on the catalyst after 9 cycles can be deduced from TGA, as compared to the fresh catalyst. As evident from Figure S14, the mass of the catalyst increased by ~19 % after recycling tests which is attributed to the amount of humins adsorbed on the catalyst surface. Removal of thus-formed humins *via* thermal decomposition remains a problem for MOFs because of their low (< 400 °C) thermal stability, and simple washing in conventional organic solvents under ultrasonic irradiation had no effect.

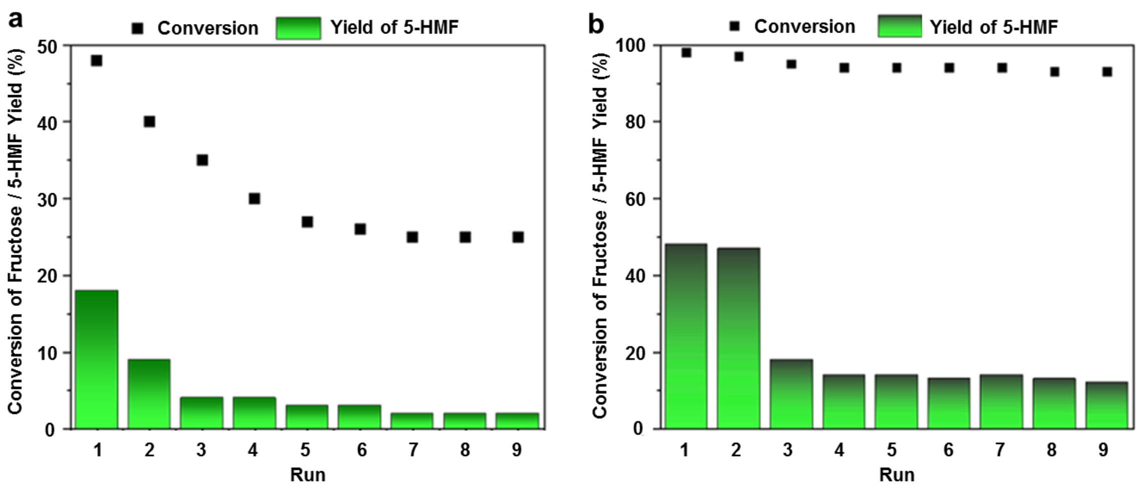

Figure 8. Conversion of fructose and yield of 5-HMF using UiO-66-SO_3H-W over several runs. Conditions: 80 ºC (a) and 100 °C (b) for 30 min.

A similar trend is observed upon recycling at 100 °C for 30 min (Figure 8.b). While the selectivity toward 5-HMF dropped significantly after the second run to reach 14 % (similar to the blank test), the fructose conversion remains almost quantitative which differs from the blank test. In parallel, the presence of an unknown compound, detected by HPLC and attributed to soluble fructose oligomers [58], increases from the second cycle. Therefore, at 100 °C the glucose conversion remains as high as ~100 % due to the combined activity of DMSO and the surface acidity of the MOF, while the inner Brønsted acidity becomes inaccessible due to humins formation. For evaluation of a catalyst's activity in fructose dehydration in DMSO it is critical to consider the solvent effect, which is negligible at 80 °C and becomes considerable at 100 °C and above. Importantly, the catalyst retained its structural integrity (Figure S15) under the given conditions even after 9 cycles which implies that the observed deactivation is not due to structural collapse of the MOF structure but rather to the lack of accessibility of the sulfonic acid groups due to the humins presence.

4. Conclusion

The direct synthesis of sulfonate-functionalized UiO-66-SO_3H nanocrystals in environmentally-friendly conditions was successfully made and applied to fructose dehydration. Replacement of hazardous and toxic DMF by water as the solvent led to an alteration of the crystal structure, switching the space group from *Fm-3m* to *Im-3*. Besides, the presence of Brønsted acidic -SO_3H groups lowered the available surface area through partial pore blocking effect by ~47 %, with a comparable effect on the pore volume (~49 %).

At 100 °C, it was shown that the UiO-66-SO_3H MOF prepared in DMF reached complete fructose conversion (> 98 %) after 2 h, barely surpassing the activity of the solvent itself, DMSO. On the other hand, the same MOF prepared in water (UiO-66-SO_3H-W) demonstrated complete fructose conversion already after 30 min under the same conditions. This catalyst showed high activity within the whole proposed range of temperatures (80-120 °C). Thus, at mild 80 °C, UiO-66-SO_3H-W demonstrated the decent

81 % fructose conversion and 52 % 5-HMF yield after 3 h while the blank test in DMSO showed no fructose conversion.

Additionally, UiO-66-SO_3H-W exhibited a well-pronounced structural stability. After 6 h of catalytic tests up to 120 °C, the catalyst retained its crystal structure. Moreover, its structural integrity was proven by performing 9 consecutive catalytic runs with no washing/drying steps between each run, simulating a continuous process with a batch reactor. The catalyst gradually lost its activity towards 5-HMF formation with the yield values dropping from 18 % to 3 %, as well as from 48 % to 14 % similar to those of the blank tests at 80 °C and 100 °C, respectively. Thus, it was shown that 80 °C is an acceptable temperature to examine a catalyst's activity without the effect of DMSO. On the other hand, frequently reported fructose conversion and 5-HMF yield at 100 °C and above should be attributed to the dual catalyst/DMSO activity.

ASSOCIATED CONTENT

Supporting Information. The Supporting Information is available free of charge at DOI: 10xxxx/xxxxx.

N_2 adsorption-desorption isotherms, SEM micrographs of MOF powders, NLDFT pore size distribution calculated from N_2 isotherms, Photographs of solutions after test, HPLC chromatograms of the solution, TGA thermographs before and after test, XPS spectrum of UiO-66, Additional XRD patterns, FTIR-ATR spectra of the powders, and catalytic results under different temperatures. The following files are available free of charge.

AUTHOR INFORMATION

Corresponding Author

*Mail: jeremy.dhainaut@univ-lille.fr.

Acknowledgements

The Chevreul Institute is thanked for its help in the development of this work through the ARCHI-CM project supported by the “Ministère de l’Enseignement Supérieur de la Recherche et de l’Innovation”, the region “Hauts-de-France”, the ERDF program of the European Union and the “Métropole Européenne de Lille”. B. Yeskendir is grateful to the Polytechnic University Hauts-de-France and the University of Lille for the PhD funding. M. Trentseaux is acknowledged for the Raman analyses. P.M. de Souza acknowledges the Région Hauts-de-France, I-SITE and MEL for the support in the frame of CatBioInnov and RECABIO projects.

REFERENCES

[1] Song, B.; Lin, R.; Ho, C.; Wu, H.; Tsui, T.; Yu, Y. Recent Advances and Challenges of Inter-Disciplinary Biomass Valorization by Integrating Hydrothermal and Biological Techniques. *Renew. Sustain. Energy Rev*. **2021**, *135*, 110370. https://doi.org/10.1016/j.rser.2020.110370.

[2] Mondelli, C.; Gozaydın, G.; Yan, N.; Perez-Ramirez, J. Biomass Valorisation over Metal-Based Solid Catalysts from Nanoparticles to Single Atoms. *Chem. Soc. Rev.* **2020**, *49*, 3764–3782. https://doi.org/10.1039/d0cs00130a.

[3] Ning, P.; Yang, G.; Hu, L.; Sun, J.; Shi, L.; Zhou, Y.; Wang, Z.; Yang, J. Biotechnology for Biofuels Recent Advances in the Valorization of Plant Biomass. *Biotechnol. Biofuels.* **2021**, *14*, 1–22. https://doi.org/10.1186/s13068-021-01949-3.

[4] Esposito, D.; Antonietti, M. Redefining Biorefinery : the Search for Unconventional Building Blocks for Materials. *Chem. Soc. Rev.* **2015**, *44*, 5821–5835. https://doi.org/10.1039/c4cs00368c.

[5] Rinaldi, R.; Schüth, F. Acid Hydrolysis of Cellulose as the Entry Point into Biorefinery Schemes. *ChemSusChem.* **2009**, *2*, 1096–1107. https://doi.org/10.1002/cssc.200900188.

[6] Kang, S.; Fu, J.; Zhang, G. From Lignocellulosic Biomass to Levulinic Acid : A Review on Acid-Catalyzed Hydrolysis. *Renew. Sustain. Energy Rev.* **2018**, *94*, 340–362. https://doi.org/10.1016/j.rser.2018.06.016.

[7] Amin, F. R.; Khalid, H.; Zhang, H.; Rahman, S.; Zhang, R.; Liu, G.; Chen, C. Pretreatment Methods of Lignocellulosic Biomass for Anaerobic Digestion. *AMB Express.* **2017**, *7*, 72. https://doi.org/10.1186/s13568-017-0375-4.

[8] Zhou, C.; Xia, X.; Lin, C.; Tong, D.; Beltramini, J. Catalytic Conversion of Lignocellulosic Biomass to Fine Chemicals and Fuels. *Chem. Soc. Rev.* **2011**, *40*, 5588–5617. https://doi.org/10.1039/c1cs15124j.

[9] Vasic-Racki, D. History of Industrial Biotransformations – Dreams and Realities, in: *Industrial Biotransformations*, 2nd ed., Wiley: Weinheim, Germany, 2006: pp. 1–36.

[10] Sajid, M.; Zhao, X.; Liu, D. Production of 2,5-Furandicarboxylic Acid (FDCA) from 5-Hydroxymethylfurfural (HMF): Recent Progress Focusing on the Chemical-Catalytic Routes. *Green Chem.* **2018**, *20*, 5427. https://doi.org/10.1039/c8gc02680g.

[11] Garcia-Lopez, E. I.; Pomilla, F. R.; Megna, B.; Testa, M. L.; Liotta, L.F.; Marci, G. Catalytic Dehydration of Fructose to 5-Hydroxymethylfurfural in Aqueous Medium over Nb_2O_5-based Catalysts. Nanomaterials **2021**, *11*, 1821. https://doi.org/10.3390/nano11071821.

[12] Wang, H.; Kong, Q.; Wang, Y.; Deng, T.; Chen, C.; Hou, X.; Zhu, Y. Graphene Oxide Catalyzed Dehydration of Fructose into 5-Hydroxymethylfurfural with Isopropanol as Cosolvent. *ChemCatChem.* **2014**, *6*, 728–732. https://doi.org/10.1002/cctc.201301067.

[13] Sayed, M.; Warlin, N.; Hulteberg, C.; Munslow, I.; Lundmark, S.; Pajalic, O.; Tunå, P.; Zhang, B.; Pyo, S.; Hatti-kaul, R. 5-Hydroxymethylfurfural from Fructose: an Efficient Continuous Process in a Water-Dimethyl Carbonate Biphasic System with High Yield Product Recovery. *Green Chem.* **2020**, *22*, 5402. https://doi.org/10.1039/d0gc01422b.

[14] Tao, F.; Song, H.; Chou, L. Dehydration of Fructose into 5-Hydroxymethylfurfural in Acidic Ionic Liquids. *RSC Adv.* **2011**, *1*, 672–676. https://doi.org/10.1039/c1ra00088h.

[15] Whitaker, M. R.; Parulkar, A.; Brunelli, N. A. Selective Production of 5-Hydroxymethylfurfural from Fructose in the Presence of an Acid-Functionalized SBA-15 Catalyst Modified with a Sulfoxide Polymer. *Mol. Syst. Des. Eng.* **2020**, *5*, 257–268. https://doi.org/10.1039/c9me00093c.

[16] Barbosa, S. L.; Freitas, M. D. S.; Santos, W. T. P.; Nelson, D. L.; Klein, S. I.; Clososki, G. C.; Caires, F. J.; Baroni, A. C. M.; Wentz, A. P. Dehydration of D-Fructose in DMSO Using a Hydrophilic Sulfonated Silica Catalyst in a Process Promoted by Microwave Irradiation. *Sci. Rep.* **2021**, *11*, 1919. https://doi.org/10.1038/s41598-020-80285-2.

[17] Huang, Z.; Pan, Y.; Chao, Y.; Shen, W.; Wang, C.; Xu, H. Triazaheterocyclic Compound as an Efficient Catalyst for Dehydration of Fructose into 5-Hydroxymethylfurfural. *RSC Adv.* **2014**, *4*, 13434. https://doi.org/10.1039/c4ra00534a.

[18] Jiang, N.; Huang, R.; Qi, W.; Su, R.; He, Z. Effect of Formic Acid on Conversion of Fructose to 5-Hydroxymethylfurfural in Aqueous/Butanol Media. *Bioenerg. Res.* **2012**, *5*, 380–386. https://doi.org/10.1007/s12155-011-9141-7.

[19] Kläusli, T. AVA Biochem: Commercialising Renewable Platform Chemical 5-HMF. *Green Process. Synth.* **2014**, *3*, 235–236. https://doi.org/10.1515/gps-2014-0029.

[20] Kruger, J. S.; Choudhary, V.; Nikolakis, V.; Vlachos, D. G. Elucidating the Roles of Zeolite H-BEA in Aqueous-Phase Fructose Dehydration and HMF Rehydration. *ACS Appl. Mater. Interfaces*. **2013**, *3*, 1279–1291. https://doi.org/10.1021/cs4002157.

[21] Qi, X.; Watanabe, M.; Aida, M.; Smith, R. L. Catalytic Dehydration of Fructose into 5-Hydroxymethylfurfural by Ion-Exchange Resin in Mixed-Aqueous System by Microwave Heating. *Green Chem.* **2008**, *10*, 799–805. https://doi.org/10.1039/b801641k.

[22] Karimi, B.; Mirzaei, H. M. The Influence of Hydrophobic/Hydrophilic Balance of

the Mesoporous Solid Acid Catalysts in the Selective Dehydration of Fructose into HMF. *RSC Adv.* **2013**, *3*, 20655. https://doi.org/10.1039/c3ra44214d.

[23] Shi, Y.; Li, X.; Hu, J.; Lu, J.; Ma, Y.; Zhang, Y.; Tang, Y. Zeolite Microspheres with Hierarchical Structures: Formation, Mechanism and Catalytic Performance. *J. Mater. Chem.* **2011**, *21*, 16223. https://doi.org/10.1039/c1jm11669j.

[24] Guo, X.; Cao, Q.; Jiang, Y.; Guan, J.; Wang, X.; Mu, X. Selective Dehydration of Fructose to 5-Hydroxymethylfurfural Catalyzed by Mesoporous SBA-15-SO_3H in Ionic Liquid BmimCl. *Carbohydr. Res.* **2012**, *351*, 35–41. https://doi.org/10.1016/j.carres.2012.01.003.

[25] Shimizu, K.; Uozumi, R.; Satsuma, A. Enhanced Production of Hydroxymethylfurfural from Fructose with Solid Acid Catalysts by Simple Water Removal Methods. *Catal. Commun.* **2009**, *10*, 1849–1853. https://doi.org/10.1016/j.catcom.2009.06.012.

[26] Morales, G.; Melero, J. A.; Paniagua, M.; Iglesias, J.; Hernández, B.; Sanz, M. Sulfonic Acid Heterogeneous Catalysts for Dehydration of C_6-Monosaccharides to 5-Hydroxymethylfurfural in Dimethyl Sulfoxide. *Chinese J. Catal.* **2014**, *35*, 644–655. https://doi.org/10.1016/S1872-2067(14)60020-6.

[27] Bavykina, A.; Kolobov, N.; Khan, I. S.; Bau, J. A.; Ramirez, A.; Gascon, J. Metal-Organic Frameworks in Heterogeneous Catalysis: Recent Progress, New Trends, and Future Perspectives. *Chem. Rev.* **2020**, *120*, 8468–8535. https://doi.org/10.1021/acs.chemrev.9b00685.

[28] Dias, E. M.; Petit, C. Towards the Use of Metal-Organic Frameworks for Water Reuse: a Review of the Recent Advances in the Field of Organic Pollutants Removal and Degradation and the Next Steps in the Field. *J. Mater. Chem. A.* **2015**, *3*, 22484–22506. https://doi.org/10.1039/C5TA05440K.

[29] Barea, E.; Montoro, C.; Navarro, J. A. R. Toxic Gas Removal – Metal-Organic Frameworks for the Capture and Degradation of Toxic Gases and Vapours. *Chem. Soc. Rev.* **2014**, *43*, 5419–5430. https://doi.org/10.1039/c3cs60475f.

[30] Shet, S. P.; Priya, S. S.; Sudhakar, K.; Tahir, M. A Review on Current Trends in Potential Use of Metal-Organic Framework for Hydrogen Storage. *Int. J. Hydrogen Energy.* **2021**, *46*, 11782–11803. https://doi.org/10.1016/j.ijhydene.2021.01.020.

[31] Datta, S. J.; Mayoral, A.; Bettahalli, N. M. S.; Bhatt, P. M.; Karunakaran, M.; Carja, I. D.; Fan, D.; Mileo, P. G. M.; Semino, R.; Maurin, G.; Terasaki, O.; Eddaoudi, M. Rational Design of Mixed-Matrix Metal-Organic Framework Membranes for Molecular Separations. *Science* **2022**, *376*, 1080-1087. https://doi.org/ 10.1126/science.abe0192.

[32] Cavka, J. H.; Jakobsen, S.; Olsbye, U.; Guillou, N.; Lamberti, C.; Bordiga, S.; Lillerud, K. P. A New Zirconium Inorganic Building Brick Forming Metal-Organic Frameworks with Exceptional Stability. *J. Am. Chem. Soc.* **2008**, *130*,

13850–13851. https://doi.org/10.1021/ja8057953.

[33] De Mello, D. M.; Tsapatsis, M. Selective Glucose to Fructose Isomerization over Modified Zirconium UiO-66 in Alcohol Media. *ChemCatChem.* **2018**, *10*, 2417–2423. https://doi.org/10.1002/cctc.201800371.

[34] Oozeerally, A. R.; Burnett, D. L.; Chamberlain, T. W.; Walton, R. I.; Degirmenci, V. Exceptionally Efficient and Recyclable Heterogeneous Metal-Organic Framework Catalyst for Glucose Isomerization in Water. *ChemCatChem.* **2018**, *10*, 706–709. https://doi.org/10.1002/cctc.201701825.

[35] Chen, J.; Li, K.; Chen, L.; Liu, R.; Huang, X.; Ye, D. Conversion of Fructose into 5-Hydroxymethylfurfural Catalyzed by Recyclable Sulfonic Acid-Functionalized Metal-Organic Frameworks. *Green Chem.* **2014**, *16*, 2490. https://doi.org/10.1039/c3gc42414f.

[36] Kim, T. H.; Kim, S. G. Clinical Outcomes of Occupational Exposure to N,N-Dimethylformamide: Perspectives from Experimental Toxicology. *Saf. Health Work.* **2011**, *2*, 97–104. https://doi.org/10.5491/SHAW.2011.2.2.97.

[37] Foo, M. L.; Horike, S.; Fukushima, T.; Hijikata, Y.; Kubota, Y.; Takata, M.; Kitagawa, S. Ligand-Based Solid Solution Approach to Stabilisation of Sulphonic Acid Groups in Porous Coordination Polymer $Zr_6O_4(OH)_4(BDC)_6$ (UiO-66). *Dalt. Trans.* **2012**, *41*, 13791–13794. https://doi.org/10.1039/c2dt31195j.

[38] Biswas, S.; Zhang, J.; Li, Z.; Liu, Y.; Grzywa, M.; Sun, L.; Volkmer, D.; Van Der Voort, P. Enhanced Selectivity of CO_2 over CH_4 in Sulphonate-, Carboxylate- and Iodo-Functionalized UiO-66 Frameworks. *Dalt. Trans.* **2013**, *42*, 4730–4737. https://doi.org/10.1039/c3dt32288b.

[39] Piscopo, C. G.; Polyzoidis, A.; Schwarzer, M.; Loebbecke, S. Stability of UiO-66 under Acidic Treatment: Opportunities and Limitations for Post-Synthetic Modifications. *Microporous Mesoporous Mater.* **2015**, *208*, 30–35. https://doi.org/10.1016/j.micromeso.2015.01.032.

[40] Reinsch, H. "Green" Synthesis of Metal-Organic Frameworks. *Eur. J. Inorg. Chem.* **2016**, *2016*, 4290–4299. https://doi.org/10.1002/ejic.201600286.

[41] Zhang, J.; White, G.; Ryan, M.; Hunt, A. J.; Katz, M. J. Dihydrolevoglucosenone (Cyrene) as a Green Alternative to N,N-Dimethylformamide (DMF) in MOF Synthesis. *ACS Sustain. Chem. Eng.* **2016**, *4*, 7186–7192. https://doi.org/10.1021/acssuschemeng.6b02115.

[42] Khabzina, Y.; Dhainaut, J.; Ahlhelm, M.; Richter, H.; Reinsch, H.; Stock, N.; Farrusseng, D. Synthesis and Shaping Scale-up Study of Functionalized UiO-66 MOF for Ammonia Air Purification Filters. *Ind. Eng. Chem. Res.* **2018**, *57*, 8200–8208. https://doi.org/10.1021/acs.iecr.8b00808.

[43] Avci-Camur, C.; Perez-Carvajal, J.; Imaz, I.; Maspoch, D. Metal Acetylacetonates as a Source of Metals for Aqueous Synthesis of Metal-Organic Frameworks. *ACS*

Sustain. Chem. Eng. **2018**, *6*, 14554–14560. https://doi.org/10.1021/acssuschemeng.8b03180.

[44] Dai, S.; Nouar, F.; Zhang, S.; Tissot, A.; Serre, C. One-Step Room-Temperature Synthesis of Metal(IV) Carboxylate Metal-Organic Frameworks. *Angew. Chem. Int. Ed.* **2021**, *60*, 4282–4288. https://doi.org/10.1002/anie.202014184.

[45] Chen, Z.; Wang, X.; Noh, H.; Ayoub, G.; Peterson, G. W.; Buru, C. T.; Islamoglu, T.; Farha, O. K. Scalable, Room Temperature, and Water-Based Synthesis of Functionalized Zirconium-Based Metal-Organic Frameworks for Toxic Chemical Removal. *CrystEngComm.* **2019**, *21*, 2409–2415. https://doi.org/10.1039/c9ce00213h.

[46] Reinsch, H.; Bueken, B.; Vermoortele, F.; Stassen, I.; Lieb, A.; Lillerud, K.; De Vos, D. Green Synthesis of Zirconium-MOFs. *CrystEngComm.* **2015**, *17*, 4070. https://doi.org/10.1039/c5ce00618j.

[47] Hu, Z.; Peng, Y.; Kang, Z.; Qian, Y.; Zhao, D. A Modulated Hydrothermal (MHT) Approach for the Facile Synthesis of UiO-66-Type MOFs. *Inorg. Chem.* **2015**, *54*, 4862–4868. https://doi.org/10.1021/acs.inorgchem.5b00435.

[48] Chen, Z.; Wang, X.; Islamoglu, T.; Farha, O. K. Green Synthesis of a Functionalized Zirconium-Based Metal-Organic Framework for Water and Ethanol Adsorption. *Inorganics.* **2019**, *7*, 56.

[49] Taylor, J. M.; Komatsu, T.; Dekura, S.; Otsubo, K.; Takata, M.; Kitagawa, H. The Role of a Three Dimensionally Ordered Defect Sublattice on the Acidity of a Sulfonated Metal-Organic Framework. *J. Am. Chem. Soc.* **2015**, *137*, 11498–11506. https://doi.org/10.1021/jacs.5b07267.

[50] Kandiah, M.; Nilsen, M. H.; Usseglio, S.; Jakobsen, S.; Olsbye, U.; Tilset, M.; Larabi, C.; Quadrelli, E. A.; Bonino, F.; Lillerud K. P.; Lyon D. Synthesis and Stability of Tagged UiO-66 Zr-MOFs. *Chem. Mater*. **2010**, *22*, 6632–6640. https://doi.org/10.1021/cm102601v.

[51] De Mello, M. D.; Kumar, G.; Tabassum, T.; Jain, S. K.; Chen T.-H., Caratzoulas, S.; Li, X.; Vlachos, D. G.; Han, S.; Scott, S.; Dauenhauer, P. J.; Tsapatsis, M. Phosphonate-Modified UiO-66 Brønsted Acid Catalyst and its Use in Dehydra-Decyclization of 2-Methyltetrahydrofuran to Pentadienes. *Angew. Chem. Int. Ed.* **2020**, *59*, 13260–13266. https://doi.org/10.1002/anie.202001332.

[52] Juan-Alcaniz, J.; Gielisse, R.; Lago, A. B.; Ramos-Fernandez, E. V.; Serra-Crespo, P.; Devic, T.; Guillou, N.; Serre, C.; Kapteijn, F.; Gascon J. Towards Acid MOFs – Catalytic Performance of Sulfonic Acid Functionalized Architectures. *Catal. Sci. Technol.* **2013**, *3*, 2311–2318. https://doi.org/10.1039/c3cy00272a.

[53] Hu, Z.; Peng, Y.; Gao, Y.; Qian, Y.; Ying, S.; Yuan, D.; Horike, S.; Ogiwara, N.; Babarao, R.; Wang, Y.; Yan, N.; Zhao, D. Direct Synthesis of Hierarchically Porous Metal-Organic Frameworks with High Stability and Strong Brønsted Acidity: The Decisive Role of Hafnium in Efficient and Selective Fructose

Dehydration. *Chem. Mater.* **2016**, *28*, 2659–2667. https://doi.org/10.1021/acs.chemmater.6b00139

[54] Hasan, Z.; Khan, N. A.; Jhung, S. H. Adsorptive Removal of Diclofenac Sodium from Water with Zr-Based Metal-Organic Frameworks. *Chem. Eng. J.* **2015**, *284*, 1406–1413. https://doi.org/10.1016/j.cej.2015.08.087.

[55] Chavan, S. M.; Shearer, G. C.; Svelle, S.; Olsbye, U.; Bonino, F.; Ethiraj, J.; Lillerud, K. P.; Bordiga, S. Synthesis and Characterization of Amine-Functionalized Mixed-Ligand Metal-Organic Frameworks of UiO-66 Topology. *Inorg. Chem.* **2014**, *53*, 9509–9515.

[56] Shearer, G. C.; Chavan, S.; Bordiga, S.; Svelle, S.; Olsbye, U.; Lillerud, K. P. Defect Engineering: Tuning the Porosity and Composition of the Metal-Organic Framework UiO-66 via Modulated Synthesis. *Chem. Mater.* **2016**, *28*, 3749–3761. https://doi.org/10.1021/acs.chemmater.6b00602.

[57] Melero, J. A.; Bautista, L. F.; Iglesias, J.; Morales, G.; Sánchez-Vásquez, R.; Wilson, K.; Lee, A. F. New Insights in the Deactivation of Sulfonic Modified SBA-15 Catalysts for Biodiesel Production from Low-grade Oleaginous Feedstock. *Appl. Catal. A: General.* **2014**, *488*, 111-118. https://doi.org/10.1016/j.apcata.2014.09.023.

[58] Kılıc, E.; Yılmaz, S. Fructose Dehydration to 5-Hydroxymethylfurfural over Sulfated TiO_2−SiO_2, Ti-SBA-15, ZrO_2, SiO_2, and Activated Carbon Catalysts. *Ind. Eng. Chem. Res.* **2015**, *54*, 5220–5225. https://doi.org/10.1021/acs.iecr.5b00628.

[59] Sengwa, R. J.; Sankhla, S.; Khatri, V. Dielectric Characterization and Molecular Interaction Behaviour in Binary Mixtures of Amides with Dimethylsulphoxide and 1,4-Dioxane. *J. Mol. Liq.* **2010**, *151*, 17–22. https://doi.org/10.1016/j.molliq.2009.10.011.

[60] Fachri, B. A.; Abdilla, R.; Bovenkamp, H.; Rasrendra, C.; Heeres H. J. Experimental and Kinetic Modeling Studies on the Sulphuric Acid Catalyzed Conversion of D-Fructose to 5-Hydroxymethylfurfural and Levulinic acid in Water. *ACS Sustain. Chem. Eng.* **2015**, *3,* 3024–3034. https://doi.org/10.1021/acssuschemeng.5b00023.

[61] Tsilomelekis, G.; Orella, M. J.; Lin, Z.; Cheng, Z.; Zheng, W.; Nikolakis, V.; Vlachos, D. G. Molecular Structure, Morphology and Growth Mechanisms and Rates of 5-Hydroxymethylfurfural (HMF) Derived Humins. *Green Chem.* **2016**, *18*, 1983–1993. https://doi.org/10.1039/c5gc01938a.